Quantum-kinetic study of femtosecond pump-and-probe spectra of bulk GaAs

K. Hannewald, S. Glutsch, and F. Bechstedt
Friedrich-Schiller-Universität Jena, Institut für Festkörpertheorie und Theoretische Optik, Max-Wien-Platz 1, D-07743 Jena, Germany
(Received 7 September 1999; revised manuscript received 3 November 1999)

We present quantum-kinetic calculations for pump-and-probe signals of bulk semiconductors based on the second Born approximation for electron–LO-phonon interaction. The relaxation process of laser-excited electron-hole pairs is studied along the whole frequency domain including the exciton resonance. This allows a description of carrier cooling due to LO phonons at arbitrary long time delays, from initial hole burning at the pump frequency until exciton bleaching after accumulation near the band extrema. At low temperature, a bottleneck effect is predicted for small pump intensities. At room temperature, signatures of upward scattering become visible. The numerical results for GaAs are in good qualitative agreement with recent measurements [A. Leitenstorfer *et al.*, Phys. Rev. Lett. **76**, 1545 (1996); C. Fürst *et al.*, Phys. Rev. Lett. **78**, 3733 (1997)].

I. INTRODUCTION

After the discovery of the optical Stark effect in gallium arsenide in 1986,[1] many light-induced coherent phenomena formerly known only from atomic and molecular physics have also been found in semiconductors. Important examples are the observation of photon echoes, free-induction decay, quantum beats, and, during the last two years, excitonic hyper-Raman gain,[2] self-induced transparency,[3] and Rabi oscillations.[4]

Due to short dephasing times in semiconductors, this development goes along with enormous progress in ultrafast experimental techniques. Femtosecond-laser spectroscopy has become so elaborated that even time-resolved studies of the interaction between laser-induced electron-hole pairs and lattice vibrations are now feasible.[5–7] This follows similar achievements in molecular physics, where observation and coherent control of molecule vibrations by short laser pulses has opened the intriguing prospect of light-controlled chemical reactions.

In GaAs, the relevant time scale for studying the electron-lattice interaction is given by the LO-phonon period, $T_{\mathrm{LO}} = 115$ fs. For shorter time intervals, energy transfer between electrons and lattice via emission or absorption of LO phonons cannot be described in terms of completed collisions because of the quantum-mechanical time-energy uncertainty principle. The coherent control of those scattering events was recently achieved by Wehner *et al.*[7] in a three-pulse four-wave-mixing (FWM) geometry, using 15-fs pulses. Quantum-kinetic effects were also detected in recent pump-and-probe experiments by Leitenstorfer *et al.*[5] and Fürst *et al.*,[6] who resolved the step-by-step relaxation of conduction electrons after pumping high above the fundamental gap. Violation of energy conservation for each electron–LO-phonon scattering event is clearly seen in the early time regime. For delay times larger than T_{LO} the phonon replicas in the spectra narrow to the width of the initial pump-induced signal, thus fulfilling the classical energy conservation law only in the long-time limit.

As long as biexcitonic effects are negligible,[8] the coherent effects cited in the first paragraph can be explained reasonably well on the basis of the semiconductor Bloch equations (cf. Refs. 9–11, and 4, respectively). Naturally, any description of the electron-lattice interaction needs to go beyond the Hartree-Fock theory. While a semiclassical Boltzmann equation may be sufficient for modeling the long-time evolution of the coupled system of electrons and LO phonons, only a quantum-kinetic theory correctly incorporates memory effects that are essential to describe experiments on a sub-100-fs time scale.

A number of approximation schemes for the quantum-kinetic treatment of the electron–LO-phonon interaction has been proposed in the literature. Many of them are related to the so-called second Born approximation, which can be derived using either phonon-assisted density matrices[12,13] or nonequilibrium Green functions.[14,15] Sometimes, the scattering term is simplified by using a damped free-particle approximation for the Green function, thus neglecting optical band-mixing and excitonic renormalization effects.[16–18] Recently, numerical studies beyond the second Born approximation including so-called vertex corrections have been published.[19,20]

Early numerical investigations focused on the calculation of the electron distribution function during and after pulse excitation. Non-Markovian features in the relaxation process due to phonon emission were found in the second Born approximation,[12] but also for a simplified scattering term.[16,17] Recently, the influence of vertex corrections was investigated, but the results were obtained in a one-dimensional tight-binding model, where both the electron-electron interaction and the electron-phonon interaction were treated as local.[20]

Much work has been devoted to the calculation of the linear absorption in bulk samples. The existence of an Urbach tail at room temperature was demonstrated in Ref. 17, and a polaron redshift of the exciton resonance was obtained in the second Born approximation.[19,21] Vertex corrections[19] and exciton–LO-phonon resonances[22] have been found to be less important in bulk Gallium Arsenide because of the small polaron constant.

Quantum beats with nearly LO-phonon frequency[14] and the coherent control of their amplitudes,[7] demonstrated in FWM experiments, can in principle be explained in terms of a two-level system coupled to phonons.[7,23] Good agreement with experiment was obtained for simulations based on the

second Born approximation, both for the beat frequency[14,15] and the coherent-control scenario.[13]

A particular challenge is the numerical calculation of pump-and-probe spectra. In Ref. 6, the distribution functions are first calculated in a one-dimensional band structure and then converted into differential transmission spectra (DTS) by solving the semiconductor Bloch equations. In Ref. 18, the second Born approximation with a simplified scattering term was applied. Reasonable agreement with experimental DTS signals was achieved, in the case of excitation high above the fundamental band gap. So far, no calculations of pump-and-probe signals in the second Born approximation with the correct scattering term have been presented, but a consistent treatment of Coulomb interaction both in coherent *and* scattering terms will be essential for an improved description of relaxation processes. Coulomb-enhancement effects in the scattering term are known to accelerate the relaxation.[12] This is also likely to change the time evolution of pump-and-probe signals, both in the excitonic region and in the region around the phonon-related signals.

Up to now, the theoretical description of pump-and-probe experiments, including electron-phonon interaction, has concentrated on the spectral region above the band gap, where the early stages of relaxation can be monitored for short-time delays. However, with increasing time, electrons and holes accumulate at the band extrema. This results in strong exciton bleaching, as seen in the experiment.[5] Therefore, a description of the complete relaxation process due to phonons requires calculations that are accurate at all spectral regions. From the numerical point of view, this entails a dense grid and a large domain in energy space, in order to account equally for bound and continuum states. Since the signal has to be computed up to very long times, a fast numerical algorithm is essential.

This paper aims to present a consistent description of excitation and subsequent relaxation of laser-induced nonequilibrium electron-hole pairs, on the basis of the second Born approximation, where Coulomb interaction is incorporated both in the coherent *and* in the scattering term. This approach allows us to treat arbitrary excitation conditions, from pumping below the exciton resonance up to excitation high in the conduction band. The influence of the pump parameters and temperature will be discussed for the electron relaxation and pump-and-probe spectra. The *complete* relaxation process of the initially hot electrons is studied until the electrons reach the bottom of the conduction band. We present calculations for pump-and-probe spectra of bulk GaAs, where the signatures of this cooling process can be directly monitored along the whole spectral region. The analysis is based upon a stable, very efficient, and highly accurate numerical algorithm. We show that consequences due to the exact versus simplified treatment of scattering are generally small, but not negligible for experiments with small time delays. In the zero temperature case, the validity limits of the semiconductor Bloch equations without electron-phonon coupling will also be investigated.

The paper is organized as follows. In Sec. II, we introduce the basic equations of the coupled electron-phonon system, and give a brief outline of the numerical implementation. In Sec. III, we present and discuss results for both electron distribution functions and pump-and-probe spectra, using different approximation schemes and a large variety of pump parameters. A summary is given in Sec. IV.

II. BASIC EQUATIONS AND NUMERICAL IMPLEMENTATION

The density matrix of a photoexcited two-band semiconductor is defined as the expectation value of a product of electron creation and annihilation operators,

$$(n_{\mathbf{k}})_{\alpha\beta}=\langle(\hat{n}_{\mathbf{k}})_{\alpha\beta}\rangle,\quad(\hat{n}_{\mathbf{k}})_{\alpha\beta}=\hat{a}^{\dagger}_{\beta\mathbf{k}}\hat{a}_{\alpha\mathbf{k}}, \tag{1}$$

where $\alpha,\beta=c,v$ are the band indices, and $\mathbf{k}$ are the Bloch wave vectors. The diagonal elements of the density matrix (1) represent the electron distribution functions in the conduction and valence bands, whereas the nondiagonal elements are related to the (macroscopic) polarization,

$$P(t)=\frac{\mu^*}{\Omega}\sum_{\mathbf{k}}(n_{\mathbf{k}})_{cv}(t),$$

where μ and Ω are the dipole matrix element of the optical transition and the normalization volume, respectively.

The equation of motion for the density matrix (1) is governed by the Hamiltonian $\hat{H}$ via the von Neumann equation

$$i\hbar\frac{\partial}{\partial t}(n_{\mathbf{k}})_{\alpha\beta}=\langle[(\hat{n}_{\mathbf{k}})_{\alpha\beta},\hat{H}]\rangle. \tag{2}$$

The initial condition at $t=-\infty$ is given by $(n_{\mathbf{k}})^{(0)}_{\alpha\beta}=\mathrm{diag}(0,1)$, which means that the valence band is completely filled and the conduction band is empty before the arrival of the pump pulse. We consider a Hamiltonian of the form

$$\hat{H}=\hat{H}_{\mathrm{HF}}+\hat{H}_{\mathrm{ph}}+\hat{H}_{\text{el-ph}}, \tag{3}$$

where $\hat{H}_{\mathrm{HF}}$ contains the Hamiltonian of the electrons, the electron-light interaction, and the Hartree-Fock contribution of the electron-electron interaction, $\hat{H}_{\mathrm{ph}}$ is the Hamiltonian of the LO phonons, and $\hat{H}_{\text{el-ph}}$ represents the Fröhlich interaction between electrons and LO phonons. Coulomb effects beyond the mean-field approximation are neglected. Recently, the effect of Coulomb correlations[8] and vertex corrections[20] were studied for low-dimensional model systems. For bulk materials, the resulting equations of motion including these contributions do not possess spherical symmetry, which would result in a drastic increase of the numerical effort. In order to study bulk GaAs, it is essential to retain the spherical symmetry in the equations. This can be achieved if the Coulomb interaction is treated in the Hartree-Fock approximation from the very beginning, which will result in the so-called second Born approximation.

Introducing LO-phonon annihilation (creation) operators $\hat{b}^{(\dagger)}_{\mathbf{q}}$ with wave vectors $\mathbf{q}$, the three parts of the Hamiltonian (3) read, explicitly,

$$\hat{H}_{\mathrm{HF}}=\sum_{\alpha\beta\mathbf{k}}(H_{\mathbf{k}})_{\alpha\beta}\hat{a}^{\dagger}_{\alpha\mathbf{k}}\hat{a}_{\beta\mathbf{k}}, \tag{4}$$

$$(H_{\mathbf{k}})_{\alpha\beta}=\begin{pmatrix} E_c(\mathbf{k}) & -\mu E(t) \\ -\mu^* E^*(t) & E_v(\mathbf{k}) \end{pmatrix} - \frac{1}{\Omega}\sum_{\mathbf{k}'} V_{\mathbf{k}-\mathbf{k}'}[(n_{\mathbf{k}'})_{\alpha\beta}-(n_{\mathbf{k}'})^{(0)}_{\alpha\beta}],$$

$$V_{\mathbf{k}}=\frac{e^2}{\varepsilon_0\varepsilon_\infty k^2}, \tag{5}$$

$$\hat{H}_{\mathrm{ph}}=\hbar\omega_{\mathrm{LO}}\sum_{\mathbf{q}}\hat{b}^\dagger_{\mathbf{q}}\hat{b}_{\mathbf{q}}, \tag{6}$$

$$\hat{H}_{\text{el-ph}}=\sum_{\alpha\mathbf{kq}} g_{\mathbf{q}}\hat{a}^\dagger_{\alpha\mathbf{k}+\mathbf{q}}\hat{a}_{\alpha\mathbf{k}}\hat{b}_{\mathbf{q}}+\mathrm{H.c.},$$

$$g^2_{\mathbf{q}}=\frac{\hbar\omega_{\mathrm{LO}}}{2\Omega}\frac{e^2}{\varepsilon_0\varepsilon_s q^2}\left(\frac{\varepsilon_s}{\varepsilon_\infty}-1\right). \tag{7}$$

The band dispersions in Eq. (5) are described by $E_{c,v}(\mathbf{k})=\pm E_g/2\pm\hbar^2k^2/(2m_{e,h})$, with effective masses $m_{e,h}$ for electrons and holes, and a direct energy gap E_g. The laser field $E(t)$ will be specified later. The quantities $\varepsilon_0=8.854\times10^{-12}$ A s/(V m) and $e=1.602\times10^{-19}$ A s are the vacuum dielectric constant and the elementary charge, respectively. The screening of the Coulomb interaction due to interband transitions beyond the two-band model is accounted for by a static *electronic* dielectric constant ε_∞. Dynamical screening effects due to excited electron-hole pairs are neglected, this topic is currently subject of intense research.[24] The lattice part of the screening is explicitly taken into account via the electron–LO-phonon coupling (7), where ε_s is the static dielectric constant of electrons *and* lattice. The LO-phonon branch in the vicinity of the Γ point is assumed to be flat, resulting in a constant LO-phonon frequency ω_{LO}.

Inserting Eqs. (4)–(7) into the von Neumann equation (2), the density matrix becomes coupled to phonon-assisted density matrices of arbitrary order, resulting in an infinite hierarchy of differential equations. The truncation of this set of equations can be carried out either dynamics-controlled[25] or correlation-controlled.[26] In the latter approach a closed set of equations can be obtained for the density matrix $(n_{\mathbf{k}})_{\alpha\beta}$ [Eq. (1)], the (one-)phonon-assisted density matrix

$$(R_{\mathbf{kk}'})_{\alpha\beta}=\frac{1}{g_{\mathbf{k}-\mathbf{k}'}}\langle\hat{a}^\dagger_{\beta\mathbf{k}}\hat{a}_{\alpha\mathbf{k}'}\hat{b}_{\mathbf{k}-\mathbf{k}'}\rangle, \tag{8}$$

and the phonon occupation number N. If the lattice is assumed to be at thermal equilibrium, i.e.,

$$N=\frac{1}{e^{(\hbar\omega_{\mathrm{LO}}/k_BT)}-1} \tag{9}$$

(T is the temperature and k_B the Boltzmann constant), the equations of motion for $n_{\mathbf{k}}$ and $R_{\mathbf{kk}'}$ can be written as

$$i\hbar\frac{\partial}{\partial t}n_{\mathbf{k}}=[H_{\mathbf{k}},n_{\mathbf{k}}]+i\hbar\frac{\partial}{\partial t}n_{\mathbf{k}}\bigg|_{\mathrm{relax}}, \tag{10}$$

$$i\hbar\frac{\partial}{\partial t}n_{\mathbf{k}}\bigg|_{\mathrm{relax}}=\sum_{\mathbf{k}'} g^2_{\mathbf{k}-\mathbf{k}'}[R_{\mathbf{kk}'}-R_{\mathbf{k}'\mathbf{k}}+R^\dagger_{\mathbf{k}'\mathbf{k}}-R^\dagger_{\mathbf{kk}'}], \tag{11}$$

$$i\hbar\frac{\partial}{\partial t}R_{\mathbf{kk}'}=H_{\mathbf{k}'}R_{\mathbf{kk}'}-R_{\mathbf{kk}'}H_{\mathbf{k}}+\hbar\omega_{\mathrm{LO}}R_{\mathbf{kk}'} +(1-n_{\mathbf{k}'})n_{\mathbf{k}}(1+N)-n_{\mathbf{k}'}(1-n_{\mathbf{k}})N. \tag{12}$$

This set of differential equations is usually referred to as the second Born approximation. It was first successfully applied by Schilp *et al.*[12] to the calculation of the electron relaxation after pumping high above the band gap, and later to the calculation of FWM signals.[13–15] These equations can also be derived within the framework of nonequilibrium Green functions if the generalized Kadanoff-Baym ansatz is exploited.[15,16]

The representation used in Eqs. (10)–(12) allows an intuitive physical interpretation. The coherent part of Eq. (10) is given by the usual semiconductor Bloch equations,[9] or optical Bloch equations if the Coulomb term in $H_{\mathbf{k}}$ is neglected. It is supplemented by the relaxation term (11), which allows for the electron-phonon interaction via the phonon-assisted density matrix. The source term of Eq. (12) can be related to (spontaneous and induced) downward scattering and (induced) upward scattering. The corresponding products of occupation numbers are familiar from semiclassical scattering theory, except that they are now replaced by matrices. The homogeneous part of Eq. (12) describes the energy transfer related to those scattering events.

The scattering term is complicated due to the self-consistent inclusion of excitation effects and Coulomb interaction of excited electron-hole pairs. Therefore, sometimes approximations are introduced. The right-hand side of Eq. (12) can be considerably simplified by replacing the energy matrix $(H_{\mathbf{k}})_{\alpha\beta}$ with the free-particle dispersions $E_\alpha(\mathbf{k})\delta_{\alpha\beta}$, resulting in

$$i\hbar\frac{\partial}{\partial t}(R_{\mathbf{kk}'})_{\alpha\beta}=[E_\alpha(\mathbf{k}')-E_\beta(\mathbf{k})+\hbar\omega_{\mathrm{LO}}](R_{\mathbf{kk}'})_{\alpha\beta} +[(1-n_{\mathbf{k}'})n_{\mathbf{k}}(1+N)-n_{\mathbf{k}'}(1-n_{\mathbf{k}})N]_{\alpha\beta}. \tag{13}$$

In the formalism of Green functions, this amounts to substituting the exact retarded Green function in the scattering integrals by the free-particle propagator, as was done, e.g., in Refs. 16–18. We call this approach as second Born approximation with simplified scattering term. In this case, no optical band-mixing effects and excitonic renormalizations are taken into account in the relaxation term, but those effects will not only renormalize but also accelerate the scattering process. After performing the integration of Eq. (13), the scattering integral can be further simplified by taking the source term out of the scattering integral. This is called the completed collisions limit, since the history of the scatterings events is no longer taken into account. The remaining integration results in a δ function, giving rise to strict energy conservation in each electron-LO-phonon collision. If finally all off-diagonal quantities in the source term are neglected, the semiclassical Boltzmann equation is recovered.

In Sec. III, we solve the equations of motion (10)–(12)

completely. The electron distribution function is studied to extract information about the relaxation process after pumping with a laser pulse of the form $E_p(t)\exp(-i\omega_p t)$. The related pump-and-probe spectra are calculated by adding a test beam, i.e., $E(t)=E_p(t)\exp(-i\omega_p t)+cE_t(t)\exp(-i\omega_t t)$. The test beam absorption $\alpha(\omega)$ is then proportional to $\mathrm{Im}[P_t(\omega)/E_t(\omega)]$, where the contribution P_t to the total polarization P is obtained by the complex derivative

$$P_t(t)=\left.\frac{\partial P(t)}{\partial c}\right|_{c=0}=\lim_{|c|\to 0}\frac{P(t,+|c|)-P(t,-|c|)-i[P(t,+i|c|)-P(t,-i|c|)]}{4|c|}.$$

(The signal in FWM direction would correspond to the complex derivative with respect to c^*, and could be obtained by changing just one sign in the numerical routine.)

Damping of the phonon-assisted density matrix in Eq. (12) is an important issue. Sometimes, it is argued that a self-consistent damping has to be introduced in order to ensure numerical stability.[15,27] However, by comparison of self-consistent and constant damping, we find that the results are rather insensitive to the details of the damping.

At room temperature, the LO-phonon bath gives rise to a finite linewidth of the exciton. In contrast, at zero temperature, a dephasing of the microscopic polarization $(n_{\mathbf{k}})_{cv}$ has to be introduced in order to obtain a finite homogeneous broadening. Therefore, in order to minimize the number of parameters, all calculations were performed including a dephasing constant ϵ in Eq. (11) and the same damping constant ϵ in Eq. (12).

For the explicit calculations we used GaAs parameters $E_g=1.520$ eV, $m_e=0.067m_0$, $m_h=0.442m_0$, $\epsilon=0.94$ meV, $\hbar\omega_{\mathrm{LO}}=36$ meV, $\varepsilon_\infty=11.1$, and $\varepsilon_s=13.1$. The resulting exciton binding energy is 1 Ry*$=4.7$ meV. For the pump-and-probe signals, both pulses are co-circularly polarized and assumed to be Gaussian. Pulse lengths are referred to the full width at half maximum (FWHM). The test pulse parameters are fixed at a length of 15 fs and a laser intensity of $I\approx 2$ W/cm^2 ($\mu E_{t\,\max}=2\times10^{-4}$ Ry*). The pump detuning $\hbar\omega_p-E_g$ is varied between -28.2 meV (-6 Ry*) and $+112.8$ meV (24 Ry*), with a maximum intensity of $I_p=55$ MW/cm^2 ($\mu E_{p\,\max}=1$ Ry*) and the pulse lengths are between 20 and 320 fs.

In order to numerically solve the equations of motion (10)–(12), we exploit the spherical symmetry and the wave number $k=|\mathbf{k}|$ is discretized on a mesh of 500 points with a maximum electron-hole pair energy of 1160 meV. The discretization in time is performed by the leapfrog method. A time step of 0.44 fs guarantees the stability of the algorithm. The time interval runs from -3.5 to $+3.5$ ps. By the sampling theorem, this is equivalent to a spectral resolution of 0.6 meV, in the Fourier-transformed spectra. The accuracy of the algorithm was checked by testing the convergence with respect to the number of $\mathbf{k}$ points, the mesh size, and the time step. In the phonon-free case, the analytical result for the linear absorption[28] is reproduced for energies up to 140 meV (30 Ry*) above the band gap, thus taking equally into account bound and continuum states. In order to save computing time, a vectorized version of the numerical algorithm was implemented. The calculation of one pump-and-probe signal takes about 20 h on a PC with a 450-MHz Pentium II processor, and the memory required is typically about 50-MB RAM.

III. NUMERICAL RESULTS AND DISCUSSION

A. Excitation high above the band gap

We start with the numerical solution of the equations of motion in the case of excitation high above the energy gap. The pump pulse parameters are chosen to be $\hbar\omega_p-E_g=112.8$ meV, $I_p\approx 2$ MW/cm^2, and the pulse length is 320 fs. The center of the pump pulse is taken at $t=0$. In Fig. 1, the time evolution of the electron distribution in the conduction band is shown for times $t=-70$, 0, 70, 140, 350, and 1400 fs (from top to bottom) and Fig. 2 displays pump-and-probe spectra for the same set of parameters. In order to understand the effects of the different interactions and their interplay, we present results for four different approximation schemes. We start with calculations based on the optical Bloch equations for an ensemble of two-level systems, where both the Coulomb and the electron-phonon interaction are neglected (a). Then, we add the different interactions step-by-step and present results obtained using the semiconductor Bloch equations (b), the second Born approximation with simplified scattering term (c), and the second Born approximation (d).

In Fig. 1(a), the results obtained within the optical Bloch equations allow us to study the sole influence of the pump process. The pump pulse induces an electron distribution peaked at 98.0-meV excess energy that reaches its final amplitude at about $t=300$ fs. Analogously, a hole distribution in the valence band is created at 14.8 meV (not shown). Therefore, the average energy of the laser-induced electron-hole pairs is equal to the central pump frequency ω_p, and is split up between electrons and holes according to the mass ratio $m_h/m_e=6.6$.

In Fig. 2(a), the corresponding pump-and-probe spectra show the buildup of a spectral hole centered at $\hbar\omega_p$. This effect is well known from stationary theory,[9] but there are some differences due to the finite pump-pulse length. Both the width and depth of the spectral hole are strongly influenced by the spectral width of the pulse. Only for longer and stronger pulses, spectral holes with near-zero absorption and the stationary width of $4\mu E_{p\,\max}$ are obtained. A redshift of the absorption edge, as expected from the stationary case,[9] cannot be seen by eye, it amounts to less than 0.1 meV.

In Figs. 1(b) and 2(b), we extend the model to the semiconductor Bloch equations, thus taking into account the

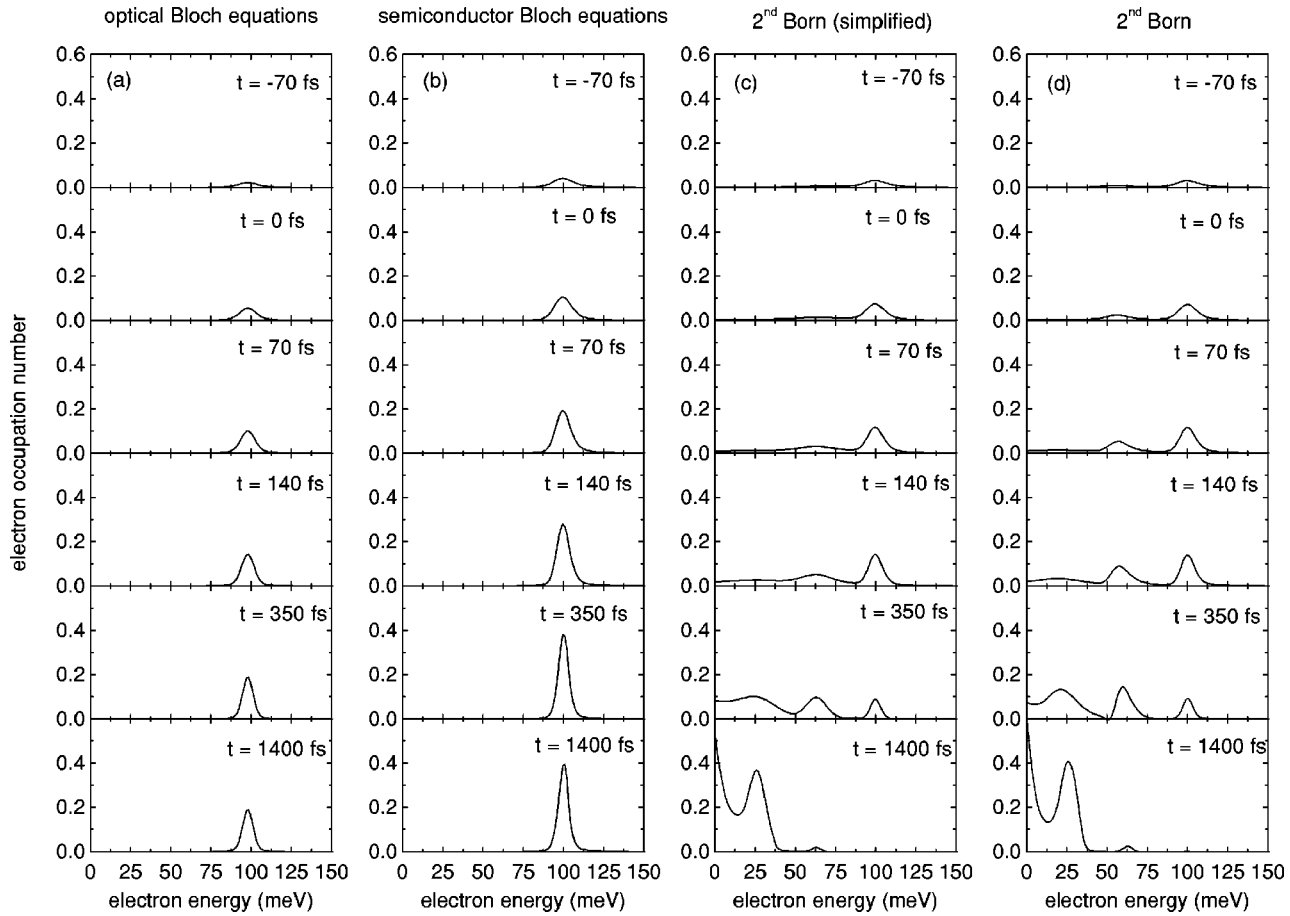

FIG. 1. Electron distribution $(n_{\mathbf{k}})_{cc}(t)$ for $t=-70$, 0, 70, 140, 350, and 1400 fs (from top to bottom). The pump parameters are $\hbar\omega_p - E_g = 112.8$ meV and $I_p \approx 2$ MW/cm^2, and the FWHM is 320 fs. From left to right: (a) theory without Coulomb interaction, (b) Hartree-Fock theory, (c) second Born approximation with simplified scattering term, and (d) second Born approximation.

Hartree-Fock terms of the Coulomb interaction between carriers. Because of band renormalization the optical transition is now given by $(H_{\mathbf{k}})_{cc}(t)-(H_{\mathbf{k}})_{vv}(t)=\hbar\omega_p$. This results in the buildup of electron-hole pairs with slightly higher *kinetic* energies, as demonstrated in Fig. 1(b), where the electron distribution is plotted as a function of energy with respect to the unrenormalized bands. The peak positions of electrons (holes) shift to 99.5 meV (15.1 meV) at $t=0$ and 100.3 meV (15.2 meV) at $t=1400$ fs. This effect is even more pronounced for stronger laser fields. The number of electron-hole pairs generated by the pulse is almost exactly doubled compared to the interaction-free case, in agreement with similar results given in Ref. 29.

In the pump-and-probe spectra of Fig. 2(b), the effects of Coulomb interaction are even more dramatic. Besides a slight bleaching and redshift (≈ 0.9 meV) of the $1s$ exciton line, the spectral region around the pump frequency does not show the line shape of a simple spectral hole. The high-energy side of the spectral hole is accompanied by an excitonic enhancement, similar to the Fermi-edge singularity. The amplitude of this edge strongly increases if the occupation numbers of electrons and holes approach the maximum value of 1, which may occur especially for excitation at lower frequencies.

In Fig. 1(c), relaxation processes due to electron–LO-phonon scattering are included via the second Born approximation with simplified scattering, according to Eq. (13). The temperature of the LO-phonon bath is taken to be zero. Phonon replicas already start to appear during the pump process. The buildup of these replicas starts from an initially broad signal that narrows with increasing time. This reflects the time-energy uncertainty principle inherent to quantum mechanics. At the early stages of each scattering event, transitions to all energies are allowed. Only for longer times does energy conservation have to be fulfilled. At $t=350$ fs, the first phonon replica has reached its maximum value which is located 36.9 meV below the initial peak. At $t=1400$ fs, the second phonon replica peaks 37.1 meV below the first one. At such long time scales, the energy transfer between the electron system and the lattice can be looked upon in terms of completed collisions, where phonons with well-defined energies are generated in the sample. In fact, the differences between the peak maxima almost perfectly fulfill the energy conservation $E_c(\mathbf{k})-E_c(\mathbf{k}')=\hbar\omega_{\mathrm{LO}}$ for intraband scattering, according to Eq. (13). Nevertheless, energetical redistribution is not yet completed. In fact, the classically expected spacing between the initial peak and the first phonon satellite is not reached until $t=2100$ fs (not shown), whereas the spacing to the second phonon satellite still remains larger than $\hbar\omega_{\mathrm{LO}}$. The peak positions at $t=2100$ fs are 98.7, 62.8, and 25.9 meV, with amplitudes of 0.0003, 0.0045, and 0.375, respectively.

Figure 2(c) shows pump-and-probe spectra within the second Born approximation with a simplified scattering term.

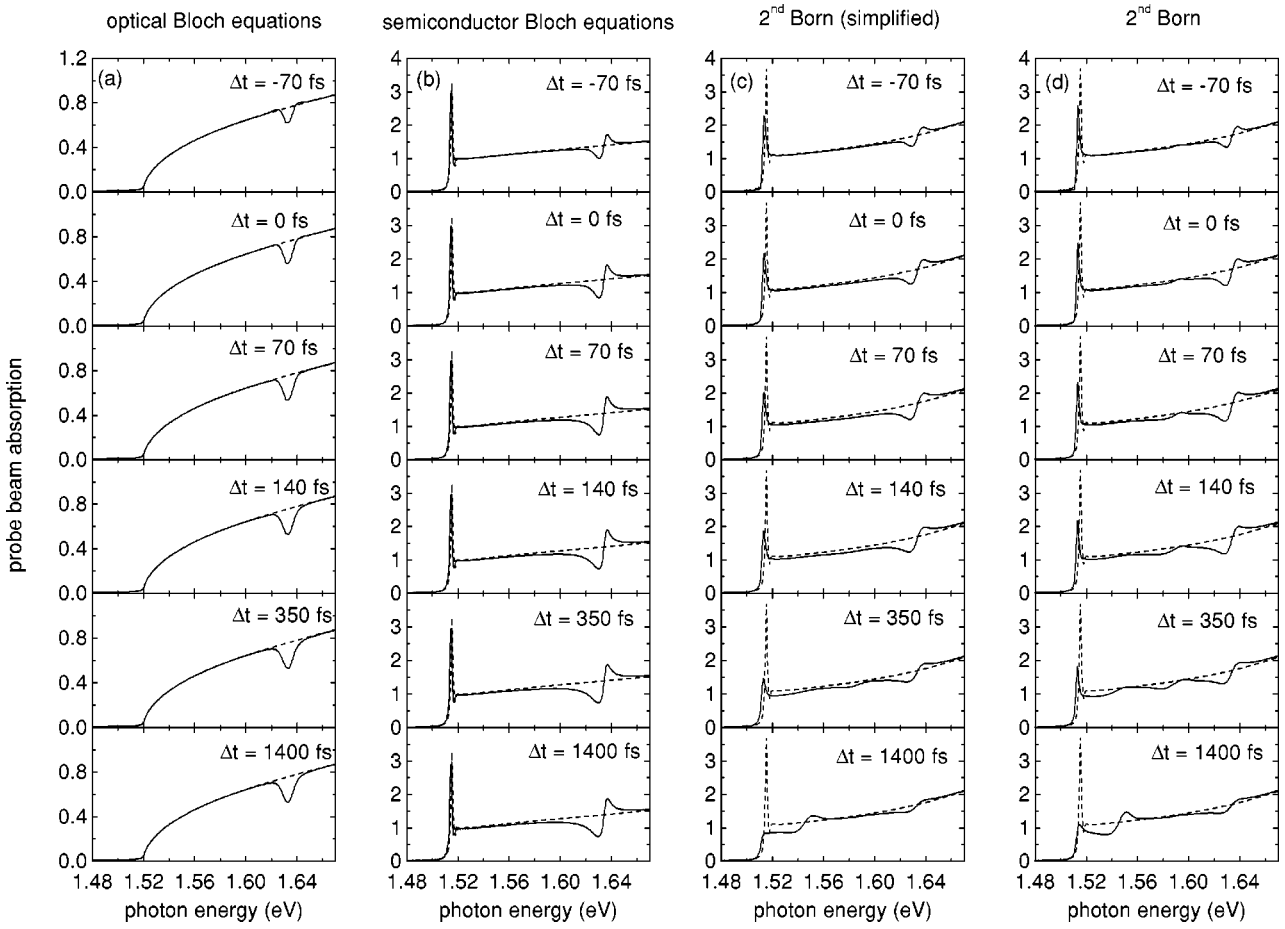

FIG. 2. Pump-and-probe spectra $\alpha(\omega)$ for $\Delta t = -70$, 0, 70, 140, 350, and 1400 fs (from top to bottom) and the same pump parameters as in Fig. 1. Dashed lines: without pump pulse, solid lines: with pump pulse. From left to right: (a) theory without Coulomb interaction, (b) Hartree-Fock theory, (c) second Born approximation with simplified scattering term, and (d) second Born approximation.

Within the same approximation, DTS signals were calculated recently by Schmenkel *et al.*,[18] but their analysis was restricted to a spectral region above the band gap, $\hbar\omega \geqslant 1.56$ eV. Here we present pump-and-probe spectra for all energies including the excitonic region, which becomes especially important for large time delays.

At negative time delays, a Fermi edge around the pump frequency appears similar to the case without phonons in Fig. 2(b). However, the exciton line is already both more strongly bleached and more strongly redshifted ($\approx$2.0 meV). For later times, Fig. 1(c) suggests the buildup of phonon replicas below the initial Fermi edge. At $\Delta t = 70$ fs, *all* energies below the initial signal show a noticeable reduction of absorption, which reflects the time-energy uncertainty principle. From $\Delta t \approx 140$ fs on, a narrow dip appears around 60 meV above the gap. It reaches its maximum depth at about 350 fs, in accordance with Fig. 1(c). Interestingly, this signal from the first phonon replica in the distribution function looks more like a spectral hole than a Fermi edge, and at no time delay is an induced absorption at its high-energy side observed. This can be attributed to the overlap with the low-energy tail of the initial Fermi edge. The same scenario repeats itself for the second phonon replica. But here, the Fermi-edge character of the signal is clearly visible at $\Delta t = 1400$ fs, which is due to the smaller overlap with the initial Fermi edge and the fact that the carriers cannot relax further.

It is worthwhile to note that the DTS signal at the first phonon replica vanishes faster than the signal around $\hbar\omega_p$, in agreement with the experiment.[5] This effect cannot be understood from the time evolution of the distribution function, where the initial peak vanishes first. This proves that after such long-time delays between pump and test pulses the system ''remembers'' the history of its excitation exclusively via the polarization that was generated in the sample by the pump pulse. In fact, if the squared polarization components $|(n_{\mathbf{k}})_{cv}(t)|^2$ at $t = 1400$ fs are plotted vs the electron-hole pair energy, the contribution at the pump position is still three orders of magnitude larger than that at the first phonon replica (not shown).

Another feature which was also seen in recent measurements[5] is found in the spectral region of the exciton. The whole relaxation process is accompanied by a gradual bleaching of the 1s exciton resonance. This results from an accumulation of the electrons (holes) in the conduction-band minimum (valence-band maximum) with increasing time. The bleaching is not complete since the relaxation runs into an LO-phonon bottleneck which will be discussed in more detail in Sec. III C.

Finally, in Figs. 1(d) and 2(d), we present results for the second Born approximation, i.e., results of a complete numerical solution of Eqs. (10)–(12). The comparison of Figs. 1(c) and 2(c) with Figs. 1(d) and 2(d) indicates that the over-

all relaxation process in both models is very similar. Therefore, we mainly concentrate on the differences.

The most significant influence of the renormalized scattering term is a faster buildup of the phonon replicas. Violation of classical energy conservation occurs only for much shorter time intervals. In Fig. 1(d), the first phonon replica has already narrowed at $t=0$, compared to the rather broad signal in Fig. 1(c). This is also observed for the second phonon replica at $t=350$ fs. Therefore, effects due to incomplete collisions are overemphasized in the simplified treatment. In the exact second Born approximation, the partial compensation of Coulomb terms in Eqs. (11) and (12) results in a more semiclassical behavior.

Another important difference is that the position of the replicas vary much stronger with time. The difference between the initial peak and the first replica decreases gradually from 43.6 meV ($t=0$) to 40.6 meV ($t=350$ fs), and in the same manner for the next replica. This spacing is considerably larger than the LO-phonon energy $\hbar\omega_{\mathrm{LO}}=36$ meV, and clearly shows the influence of the full scattering term [Eq. (12)]. Band renormalization can account for about 2 meV of the difference [cf. the discussion of Fig. 1(b)]; the rest is due to band-mixing effects in the scattering term. For later times, when most electrons are close to the band minimum, those effects are of minor importance. At $t=2100$ fs, the interaction-free spacings between all three peaks are established, with peak positions at 98.5, 62.5, and 26.4 meV, and amplitudes of 0.0003, 0.0056, and 0.405. Again, the inclusion of Coulomb effects in the scattering term leads to faster redistribution toward the classical positions.

We mention that both the faster narrowing and the stronger time dependence of the phonon replicas in the exact treatment were already observed in a pioneering work by Schilp *et al.* five years ago.[12] But at that time, the question about its experimental observability could not be answered. In Fig. 2(d), we present the first calculations, to our knowledge, for pump-and-probe signals which take these effects into account. We find two significant changes compared to the simplified treatment of the scattering term in Fig. 2(c), which could also be of experimental relevance. A pronounced dip in the spectra is already visible at $\Delta t=70$ fs, while at the same time the exciton is less bleached. This clearly reflects a more classical character of the relaxation dynamics in the exact treatment, compared to the simplified second Born approximation. This effect is especially important for comparison with DTS experiments at short time delays. Recently, the buildup of phonon-related signals was experimentally seen at delay times of less than 100 fs,[6] but could not be resolved in calculations based on the simplified second Born approximation.[18]

Another manifestation of the faster completion of collisions in the exact calculations can be seen through a better resolution of the Fermi-edge character of the phonon satellites. Interestingly, this effect is still noticeable at large time delays ($\Delta t \geqslant 1400$ fs). In contrast, the positions of the phonon-related signals do not vary significantly stronger than in the simplified calculations. This may be explained in terms of Coulomb compensation: while the distribution functions in Figs. 1(c) and 1(d) are plotted versus the kinetic energies, the test beam measures the carrier distribution (or strictly speaking, the corresponding polarization) as a function of the total energies which are much closer to each other in both models. This also explains why the overall differences between both models are relatively small.

B. Excitation at or below the band gap

As long as the pump frequency is tuned high above the band gap, we observe strong modifications in the time evolution of both the distribution functions and the spectra due to electron-phonon coupling. Because of the fast emission of LO phonons, the validity of the semiconductor Bloch equations breaks down even before the pump pulse has reached its maximum amplitude. If $\hbar\omega_p$ is situated below the threshold for LO-phonon emission, relaxation effects are still important, but mainly in the long-time limit. In pump-and-probe signals these effects show up as a gradual reduction of the initial Fermi edge combined with a pronounced bleaching of the exciton resonance.

If the pump frequency is equal to or lower than the fundamental gap, the situation changes qualitatively. In this case, inclusion of electron–LO-phonon interaction does not change the results obtained within the semiconductor Bloch equations. The distribution functions are almost identical in both approximations. Only for very long times ($t \geqslant 1400$ fs) do we find a marginal influence of the LO phonons at vanishing kinetic energies. This also holds true for the pump-and-probe spectra.

For $\hbar\omega_p - E_g = 0$ and $\Delta t = 0$, the oscillator strength of the Fermi edge strongly exceeds that of the exciton line in the linear absorption. We expect this effect to be somewhat reduced when dynamical screening is additionally taken into account, because this is exactly the spectral region, where the strongest influence of screening effects can be expected. The dominant influence of Coulomb effects under excitation at the gap is already evident from strong redistributions due to the Hartree-Fock terms. An initial shift of the peak maximum to higher kinetic energies occurs, similarly to the case of high-energy excitation in Fig. 1(b). However, a subsequent redistribution to lower energies shows that even after the pump pulse has disappeared Coulomb interaction is still effective, especially if the system is inverted, i.e., $(n_{\mathbf{k}})_{cc} > 0.5$.

C. Influence of pump intensity

In order to study the influence of the pump intensity, in Fig. 3 we compare results for in-band excitation with two different intensities, namely, for $I_p \approx 2$ MW/cm^2 (a) and $I_p \approx 20$ MW/cm^2 (b). The pulse length is fixed at 320 fs, and the pump frequency is $\hbar\omega_p - E_g = 56.4$ meV. The results do not change qualitatively for higher pump frequencies.

In Fig. 3(a), we observe the typical relaxation scenario in the low-intensity case with $I_p \leqslant 2$ MW/cm^2. The time evolution of the electron distribution shows all the features discussed in the context of Fig. 1, except for the fact that now only one LO-phonon emission is energetically allowed. Here we focus on the final state, which is reached after about 1400 fs, even though some minor redistribution is still present at later times. It is clearly seen that relaxation due to LO phonons remains incomplete. This is due to the fixed energy transfer of $\hbar\omega_{\mathrm{LO}} = 36$ meV between electrons and the lattice, which is required for completed collisions. As a conse-

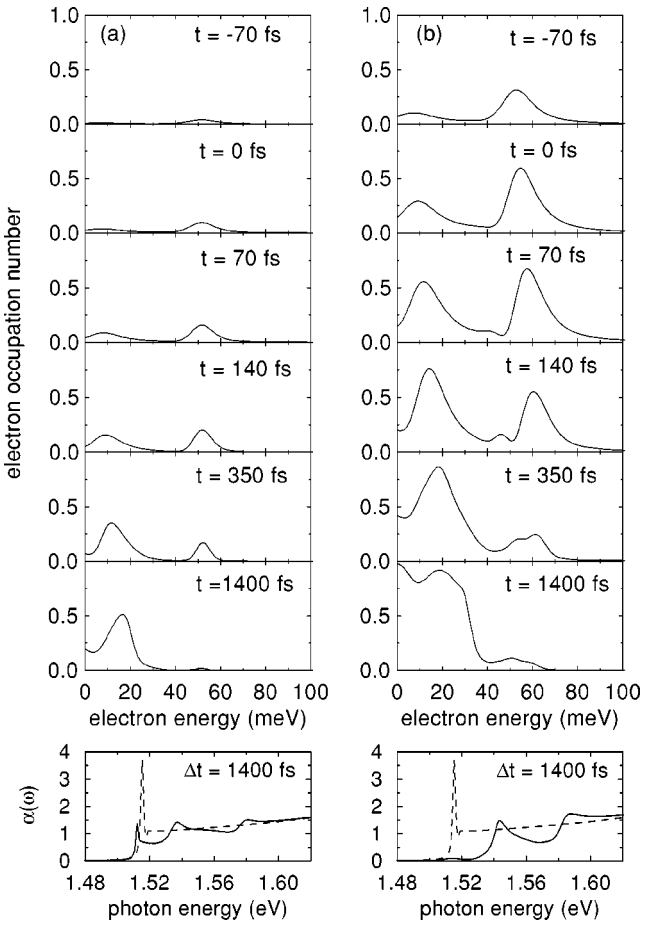

FIG. 3. Electron distribution $(n_{\mathbf{k}})_{cc}(t)$ for $t=-70$, 0, 70, 140, 350, and 1400 fs, and pump-and-probe spectra $\alpha(\omega)$ at $\Delta t=1400$ fs (from top to bottom), in the second Born approximation for different pump intensities $I_p \approx 2$ MW/cm^2 (a) and $I_p \approx 20$ MW/cm^2 (b). The other excitation parameter is $\hbar\omega_p - E_g = 56.4$ meV, and the FWHM is 320 fs.

quence, conduction electrons that have assembled at about 16.5-meV excess energy cannot emit another LO phonon. Hence the relaxation process runs into a bottleneck, where the carriers are still not thermalized, either with the lattice or within the conduction band.

Experimentally, the bottleneck effect may be observed at very low pump intensities. In this case, the carrier density is so small that Coulomb scattering between electrons is inefficient compared to LO-phonon processes. Scattering with acoustic phonons is likely to broaden the distribution function somewhat, but will be effective only on a much longer time scale, typically on the order of a few nanoseconds. We have also performed approximate calculations including electron–LA-phonon scattering, and found no significant changes on a time scale of a few picoseconds. Therefore, we expect that in this intensity regime neither Coulomb nor acoustic-phonon scattering will cancel the bottleneck effect. This opens the possibility of creating almost arbitrary nonequilibrium distributions near the band minima, up to very long times. In a pump-and-probe experiment, the bottleneck will manifest itself as a distinct (phonon-related) Fermi edge combined with an *incomplete* bleaching of the exciton, even for large time delays as demonstrated for $\Delta t=1400$ fs in Fig. 3(a).

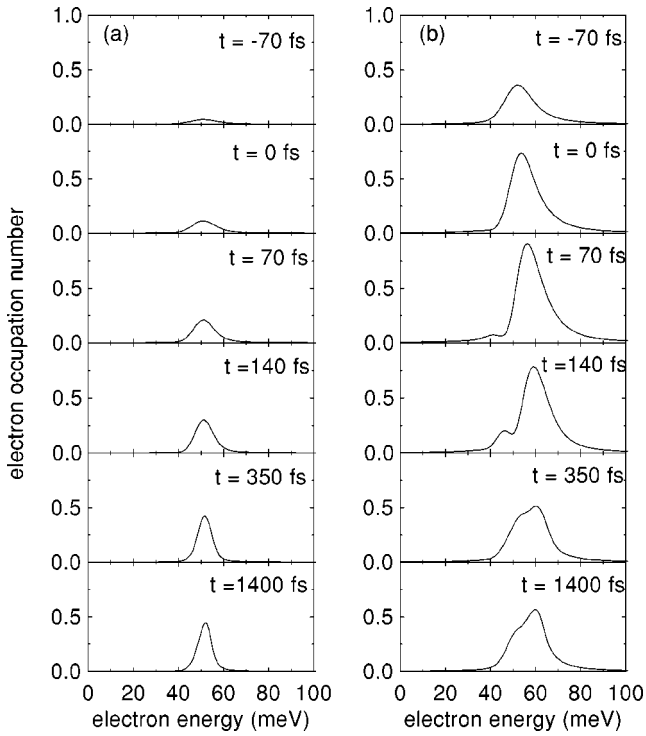

FIG. 4. Electron distribution $(n_{\mathbf{k}})_{cc}(t)$ for the same parameters as in Fig. 3, calculated using the semiconductor Bloch equations.

The picture changes completely if the pump intensity is increased. This follow from Fig. 3(b), where I_p is chosen to be ten times as high as in Fig. 3(a). In this case, we observe an almost complete thermalization of the conduction electrons at $t=1400$ fs. Finally, at $t=3500$ fs (not shown), the distribution function has evolved into a steplike function, i.e., it can be described by a Fermi distribution at zero temperature. In the pump-and-probe signal, this results in a *complete* bleaching of the exciton and continuum states up to about 8 meV above the gap. If the intensity is enhanced further ($I_p \approx 55$ MW/cm^2, not shown), continuum states with even higher energies (up to about 15 meV) are also bleached to zero absorption.

The question arises of why the relaxation due to LO phonons becomes more thermalized if I_p is increased. The answer follows directly from a comparison of the corresponding Hartree-Fock calculations in Fig. 4, where the coupling to phonons is neglected. Since the pulse length and the central pump frequency are fixed, the spectral regions of the initially created electrons are equal for both intensities. However, while in the low-intensity case Coulomb interaction leads only to small redistribution, it is much more effective at higher intensities. The larger number of electrons leads to a considerably stronger redistribution in the mean-field approximation. This results in a broadening of the carrier distribution, which is a combined effect of Coulomb interaction and phase-space filling. Compared to the low-intensity case, both low- and high-energy tails of the induced electron population are more extended. This enables electron–LO-phonon collisions into larger energy regions and thus removes the bottleneck effect. If Coulomb interactions beyond Hartree-Fock interactions, which are obviously important for a more realistic description of the high-intensity case, are taken into account, these effects would be even more pronounced, but it

is interesting to see that electron–LO-phonon scattering (in combination with Hartree-Fock terms) can suffice for a complete thermalization of conduction electrons with the lattice, despite the fixed energy transfer given by $\hbar\omega_{\mathrm{LO}}$. On the other hand, for high densities hot-phonon effects may lead to a reduction and slowing down of the carrier cooling process,[30] and should therefore also be included in more realistic studies.

D. Influence of pump pulse length

So far, we considered a pulse length of 320 fs related to a regime where one can observe the most pronounced signatures of electron–LO-phonon coupling. This is due to the fact that the spectral width of such pump pulses is smaller than the LO-phonon frequency, which improves the spectral resolution of the LO-phonon-related phenomena.

For pulse durations comparable to the LO-phonon period $T_{\mathrm{LO}}=2\pi/\omega_{\mathrm{LO}}=115$ fs (not shown), the initial pump-induced distribution and its phonon replicas begin to spectrally overlap. In the pump-and-probe signals this gives rise to an even larger extension of the low-energy tail from the initial Fermi edge, and a stronger overlap with the first phonon replica, compared to 320-fs pulses. Such effects have indeed been seen in recent experiments using 120-fs pulses.[6] Furthermore, the bottleneck effect is less dramatic because of a spectrally broader excitation. At long times, the electron distribution always evolves into a state where the peaks of the phonon replicas are smeared out. Only for high intensities does it approach the zero-temperature Fermi distribution. For low intensities, the final distribution more closely resembles a Fermi function at finite temperature, or, in other words, the carriers thermalize within the bands, but not completely with the lattice. In the pump-and-probe spectra, this can be observed again as an incomplete bleaching of the exciton, this time without a distinct (phonon-related) Fermi edge, in contrast to what is observed in Fig. 3.

If the pump pulse is chosen much shorter than T_{LO}, it will be impossible to spectrally resolve distinct phonon replicas. This is demonstrated for a 20-fs pulse in Fig. 5(a). The relaxation process can be divided into two stages. The first stage is dominated by an ultrafast redistribution toward the band minimum within less than 70 fs. This process is not related to emission of LO phonons, as becomes clear by comparison with the Hartree-Fock results in Fig. 5(b). It must therefore be attributed to effects caused by Coulomb interaction. Even at $t=140$ fs, the distribution is still reasonably well described by the semiconductor Bloch equations. Only for longer times is the influence of the phonons noticeable in Fig. 5(a) as a transfer of initially high-energy electrons toward the band minimum. During the second stage of the relaxation process, the high-energy end of the electron distribution shifts down from about 160 meV ($t=140$ fs) to about 50 meV ($t=1400$ fs) and 35 meV ($t=3500$ fs, not shown), whereas in Hartree-Fock theory it remains at about 160 meV for all times.

Recently, a quasi-instantaneous spread of the carrier population during their generation with a 30-fs pulse was measured in DTS experiments in GaAs, and attributed to quantum-kinetic carrier-carrier scattering.[31] From the Hartree-Fock results in Fig. 5(b) one could think of an easier

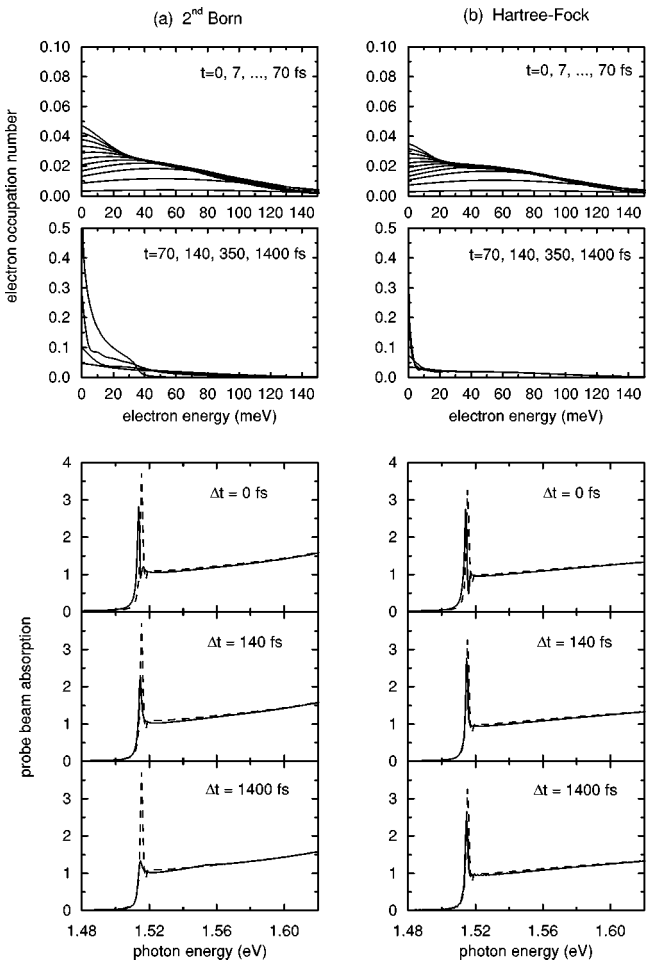

FIG. 5. Upper panels: electron distribution function $(n_{\mathbf{k}})_{cc}(t)$ at $t=0$, 7, 14, . . . , 70 fs (top), and 70, 140, 350, and 1400 fs (bottom) for pump parameters $\hbar\omega_p-E_g=56.4$ meV and $I_p\approx 20$ MW/cm^2, and a FWHM of 20 fs in the second Born approximation (a) and Hartree-Fock theory (b). Lower panels: pump-and-probe spectra $\alpha(\omega)$ at time delays $\Delta t=$ 0 (top), 140 (middle), and 1400 fs (bottom) for the same pump parameters. Dashed lines: without pump pulse, solid lines: with pump pulse.

explanation. However, in the pump-and-probe signals calculated for the same parameters, the immediate redistribution is not resolved, either in the second Born approximation [Fig. 5(a), lower panel] or in Hartree-Fock theory [Fig. 5(b), lower panel]. This is demonstrated by a comparison of the signals at $\Delta t=0$ and $\Delta t=140$ fs. For those and all intermediate time delays a spectrally broad decrease in the test beam absorption is observed, with its maximum decrease always directly at the band gap. As a result, Hartree-Fock Coulomb interaction and electron–LO-phonon scattering cannot account for the experimental observation in Ref. 31. Therefore, an explanation in terms of carrier-carrier scattering is also supported by our analysis. These effects are most likely to further amplify the ultrafast carrier-spreading, up to an order that makes its experimental observation feasible. This analysis, however, is beyond the scope of the present paper.

In contrast to the initial redistribution, the second stage of the carrier cooling can easily be followed in the pump-and-probe signals of Fig. 5(a). Including the coupling to the LO phonons, we observe a downshift of the high-energy shoulder of the pump-induced changes, combined with a continu-

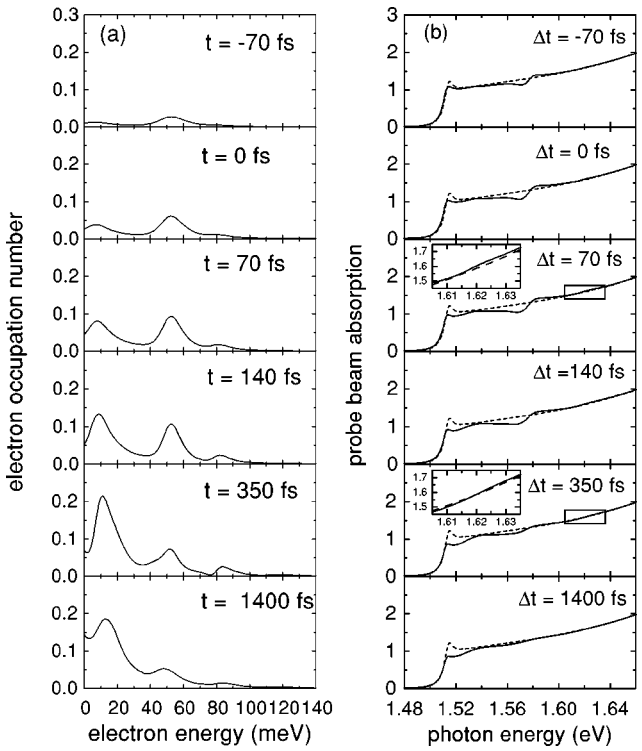

FIG. 6. Electron distribution function (a) and pump-and-probe spectra (b), including the coupling to LO phonons at room temperature for different time delays $\Delta t = -70$, 0, 70, 140, 350, and 1400 fs (from top to bottom). Pump-pulse parameters: $\hbar\omega_p - E_g = 56.4$ meV and $I_p \approx 2$ MW/cm^2, and the FWHM is 320 fs. Dashed lines: without pump pulse; solid lines: with pump pulse.

ous bleaching of the excitonic resonance, in accordance with the time evolution of the distribution function.

E. Influence of temperature

So far, all calculations were performed assuming zero temperature for the LO-phonon bath. Now we discuss the effects of finite temperatures. While for $T=0$ K only spontaneous downward scattering was possible, at finite temperatures upward scattering and induced downward scattering can also occur. From Eq. (12) it follows that the scattering rates of those processes scale linearly with the phonon number N. For low temperatures ($T \leqslant 100$ K), N is much smaller than 1, e.g., $N=0.0044$ at $T=77$ K. Therefore, the relaxation is dominated by spontaneous downward scattering. As a consequence, virtually no changes compared to the zero-temperature case are observed, either in the distribution functions, the linear absorption, or the pump-and-probe signals. In contrast, at room temperature ($T=300$ K, $N=0.33$) we observe strong deviations from the $T=0$ K picture.

In Fig. 6(a), the electron distribution at $T=300$ K is depicted for pump parameters $\hbar\omega_p - E_g = 56.4$ meV and $I_p \approx 2$ MW/cm^2, and a pulse length of 320 fs. From $t=0$ on, the buildup of a phonon replica *above* the pump-induced signal can be seen. Interestingly, the energy difference between these two peaks is much smaller than $\hbar\omega_{\mathrm{LO}}$, namely, 26.3 meV at $t=0$. On the other hand, the spacing between the pump-induced peak and the downscattering peak is larger than $\hbar\omega_{\mathrm{LO}}$, namely, 45.5 meV at $t=0$, which is almost the same value as for $T=0$ K (44.3 meV). As in the discussion of Fig. 1(d), the deviations from the LO-phonon energy can be attributed to the interplay of band renormalization and band mixing effects in Eq. (12). Only for later times do the spacings approach $\hbar\omega_{\mathrm{LO}}$. For example, at $t=1400$ fs, the peak positions are 83.8, 48.0, and 12.9 meV.

At early times ($t \leqslant 350$ fs), the downward scattering develops very similarly to the $T=0$ K scenario, which can be seen by comparison with Fig. 3(a). The only difference is that the peak amplitudes are strongly reduced due to upward-scattering processes. For later times, the electron distribution at $T=300$ K becomes much more thermalized than at zero temperature. This can already be seen at $t=1400$ fs, while at $t=3500$ fs (not shown) the peaks in the distribution function are totally smoothed out. For all other pump conditions, we also never observed a bottleneck. Hence at room temperature there is no bottleneck effect. It is removed since upward scattering is always possible. In some cases, it even causes the distribution function at zero kinetic energy to bounce back to lower values, in order to realize final thermalization.

The growing out of a high-energy population due to phonon absorption processes is also observed for excitation at or below the band gap, in agreement with previous results.[17] The question arises of whether or not this population can be experimentally observed. For this reason, in Fig. 6(b) we calculate the pump-and-probe spectra for the same parameters as in Fig. 6(a). Around $\Delta t=70$ fs a small signal above the initial Fermi edge is visible. Due to its small amplitude and the overlap with the high-energy side of the initial Fermi edge, it will appear as a small *dip* in DTS measurements. Only for larger time delays will its Fermi-edge character become clear, as demonstrated in the inset at $\Delta t=350$ fs.

The pump-and-probe spectra at large time delays show an incomplete bleaching of the exciton, while the phonon-related signals gradually disappear. The bleaching of the exciton, relative to the linear absorption, is always less pronounced than for $T=0$ K. This reflects the fact that fewer carriers can accumulate near the bottom of the conduction band due to upscattering. The disappearance of the phonon-related signatures is the result of thermalization.

Finally, we mention that all spectra at $T=300$ K exhibit an exponential Urbach tail at the low-energy side of the excitonic resonance. Similarly, this was shown for linear absorption in Ref. 17.

IV. SUMMARY

We have presented a quantum-kinetic description of pump-and-probe experiments in bulk GaAs based on the second Born approximation for electron–LO-phonon interaction, where Coulomb effects are included consistently both in coherent and scattering terms. Moreover, we calculated the signatures of hot-carrier cooling in pump-and-probe spectra including the excitonic region. This allowed us to monitor both the initial stages of relaxation due to LO phonons and the subsequent carrier accumulation near the band extrema.

For excitation high above the gap, good qualitative agreement with recent DTS measurements[5,6] is achieved, both in the spectral region above the gap and around the exciton line. An initial hole burning with Fermi-edge character, a subse-

quent buildup of phonon replicas, and a gradual exciton bleaching are observed in the experiment, and are well reproduced by theory. At large time delays, the accumulation of electrons in the band minima results in strong exciton bleaching, in agreement with the experiment.[5]

We have shown that LO-phonon effects related to the exact treatment versus the simplified treatment of the scattering term are generally small, but not negligible for experiments with short time delays. We find that only the exact second Born approximation is able to reproduce the experimental observation of phonon-related signals for $\Delta t \leqslant 100$ fs. In contrast, the simplified model is found to produce a much slower buildup of phonon satellites in the pump-and-probe signals.

We have also investigated the validity of the semiconductor Bloch equations. We have proved that for excitation at or below the band gap, results without electron-phonon coupling are equivalent to those of the second Born approximation. For pump pulses shorter than the LO-phonon period, the electron distribution is found to be reasonably well described by semiconductor Bloch equations in the early-time regime, even if the central frequency is tuned above the threshold for LO-phonon emission. In this situation, only in the long-time limit does electron-phonon scattering become dominant.

Finally, we have discussed the influence of pump parameters and the temperature. At low temperature, a phonon-bottleneck effect is predicted for pumping at low intensities above the band gap, whereas for higher intensities electron–LO-phonon scattering alone can suffice for complete thermalization with the lattice. In pump-and-probe spectra, the bottleneck results in a distinct phonon-related Fermi edge combined with an incomplete exciton bleaching, which should persist up to very large time delays. At finite temperatures, upward scattering is predicted to become visible in pump-and-probe experiments.

ACKNOWLEDGMENTS

The authors are indebted to M. Herbst and P. Lipavsky for interesting discussions and for communicating information prior to publication. This work was supported by the Thüringer Ministerium für Wissenschaft, Forschung und Kultur.

[1] A. Mysyrowicz, D. Hulin, A. Antonetti, A. Migus, W. T. Masselink, and H. Morkoç, Phys. Rev. Lett. **56**, 2748 (1986).
[2] J.-P. Likforman, M. Joffre, and D. Hulin, Phys. Rev. Lett. **79**, 3716 (1997); J.-P. Likforman, D. Hulin, and M. Joffre, Phys. Status Solidi B **206**, 71 (1998).
[3] H. Giessen, A. Knorr, S. Haas, S. W. Koch, S. Linden, J. Kuhl, M. Hetterich, M. Grün, and C. Klingshirn, Phys. Rev. Lett. **81**, 4260 (1998).
[4] A. Schülzgen, R. Binder, M. E. Donovan, M. Lindberg, K. Wundke, H. M. Gibbs, G. Khitrova, and N. Peyghambarian, Phys. Rev. Lett. **82**, 2346 (1999).
[5] A. Leitenstorfer, C. Fürst, A. Laubereau, W. Kaiser, G. Tränkle, and G. Weimann, Phys. Rev. Lett. **76**, 1545 (1996).
[6] C. Fürst, A. Leitenstorfer, A. Laubereau, and R. Zimmermann, Phys. Rev. Lett. **78**, 3733 (1997); A. Leitenstorfer, C. Fürst, A. Laubereau, and R. Zimmermann, Phys. Status Solidi B **204**, 300 (1997).
[7] M. U. Wehner, M. H. Ulm, D. S. Chemla, and M. Wegener, Phys. Rev. Lett. **80**, 1992 (1998); M. U. Wehner, D. S. Chemla, and M. Wegener, Phys. Rev. B **58**, 3590 (1998); M. U. Wehner, M. H. Ulm, D. S. Chemla, and M. Wegener, Phys. Status Solidi B **206**, 281 (1998).
[8] C. Sieh, T. Meier, F. Jahnke, A. Knorr, S. W. Koch, P. Brick, M. Hübner, C. Ell, J. Prineas, G. Khitrova, and H. M. Gibbs, Phys. Rev. Lett. **82**, 3112 (1999).
[9] S. Schmitt-Rink and D. S. Chemla, Phys. Rev. Lett. **57**, 2752 (1986); S. Schmitt-Rink, D. S. Chemla, and H. Haug, Phys. Rev. B **37**, 941 (1988).
[10] K. Hannewald, S. Glutsch, and F. Bechstedt, Phys. Rev. B **58**, 15 336 (1998).
[11] S. W. Koch, A. Knorr, R. Binder, and M. Lindberg, Phys. Status Solidi B **173**, 177 (1992).
[12] J. Schilp, T. Kuhn, and G. Mahler, Phys. Rev. B **50**, 5435 (1994).
[13] V. M. Axt, M. Herbst, and T. Kuhn, Superlatt. Microstruct. **26**, 117 (1999).
[14] L. Bányai, D. B. Tran Thoai, E. Reitsamer, H. Haug, D. Steinbach, M. U. Wehner, M. Wegener, T. Marschner, and W. Stolz, Phys. Rev. Lett. **75**, 2188 (1995).
[15] L. Bányai, E. Reitsamer, D. B. Tran Thoai, and H. Haug, J. Opt. Soc. Am. B **13**, 1278 (1996).
[16] H. Haug, Phys. Status Solidi B **173**, 139 (1992); L. Bányai, D. B. Tran Thoai, C. Remling, and H. Haug, *ibid.* **173**, 149 (1992).
[17] D. B. Tran Thoai and H. Haug, Phys. Rev. B **47**, 3574 (1993).
[18] A. Schmenkel, L. Bányai, and H. Haug, J. Lumin. **76&77**, 134 (1998).
[19] Th. Östreich, Phys. Status Solidi A **164**, 313 (1997); Th. Östreich, N. Donlagic, C. Wöhler, and K. Schönhammer, Phys. Status Solidi B **206**, 205 (1998).
[20] N. Donlagic and Th. Östreich, Phys. Rev. B **59**, 7493 (1999).
[21] E. Binder, J. Schilp, and T. Kuhn, Phys. Status Solidi B **206**, 227 (1998).
[22] R. Zimmermann and C. Trallero-Giner, Phys. Rev. B **56**, 9488 (1997).
[23] H. Castella and R. Zimmermann, Phys. Rev. B **59**, 7801 (1999).
[24] Q. T. Vu, L. Bányai, H. Haug, F. X. Camescasse, J.-P. Likforman, and A. Alexandrou, Phys. Rev. B **59**, 2760 (1999).
[25] V. M. Axt and S. Mukamel, Rev. Mod. Phys. **70**, 145 (1998).
[26] J. Fricke, Ann. Phys. (N.Y.) **252**, 479 (1996).
[27] H. Haug and A.-P. Jauho, *Quantum Kinetics in Transport and Optics of Semiconductors* (Springer, Berlin, 1996).
[28] R. J. Elliott, Phys. Rev. **108**, 1384 (1957).
[29] R. Binder, S. W. Koch, M. Lindberg, N. Peyghambarian, and W. Schäfer, Phys. Rev. Lett. **65**, 899 (1990).
[30] J. Schilp, T. Kuhn, and G. Mahler, Phys. Status Solidi B **188**, 417 (1995).
[31] S. Bar-Ad, P. Kner, M. V. Marquezini, D. S. Chemla, and K. El Sayed, Phys. Rev. Lett. **77**, 3177 (1996).